Authors' accepted manuscript.
Article published in *Materials Science and Engineering: C*, Volume 100, July 2019, Pages 715-723
The final published version is available at https://doi.org/10.1016/j.msec.2019.03.023

Accepted by Material Engineering C., March 2019

Towards Compliant Small-Diameter Vascular Grafts: Predictive Analytical Model and Experiments

Bouchet Mélusine*[1,2,3] Gauthier Matthieu*[3]; Maire Marion[1,2]; Ajji Abdellah[&3,4]; Lerouge Sophie[&1,2]

[1]Department of Mechanical Engineering, École de technologie supérieure (ÉTS), Montreal, QC, H3C 1K3, Canada

[2]Laboratory of Endovascular Biomaterials (LBeV), Research Centre, Centre Hospitalier de l'Université de Montréal (CRCHUM), Montreal, QC, H2X 0A9, Canada

[3]CREPEC, Department of Chemical Engineering, École Polytechnique de Montréal, Montreal, QC, H3C 3A7, Canada

[4]Institute of Biomedical Engineering, École Polytechnique de Montréal, Montreal, QC, H3C 3A7, Canada

*: Equivalent contribution to the work

&: Co-corresponding author

Corresponding authors:

Sophie Lerouge, P. Eng., PhD
Laboratory for Endovascular Biomaterials (LBeV)
CHUM Research Center (CHUM)
900 St. Denis Street
Montreal, QC, H2X 0A9, Canada
Tel: +1-514-890-8000 #28821; Fax: +1-514-412-7785
E-mail: sophie.lerouge@etsmtl.ca

Abdellah Ajji, P. Eng., PhD
CREPEC,
Department of Chemical Engineering,
École Polytechnique de Montréal,
PO Box 6079, Station Centre-Ville,
Montréal, QC, H3C 3A7, Canada Tel: +1-514-340-4711 #3703; Fax: +1-514-340-4159
E-mail: abdellah.ajji@polymtl.ca

Keywords

Vascular grafts; analytical model; electrospinning; compliance; burst pressure; permeability.

Abstract

The search for novel, more compliant vascular grafts for the replacement of blood vessels is ongoing, and predictive tools are needed to identify the most promising biomaterials. A simple analytical model was designed that enables the calculation of the ratio between the ultimate stress (σ_{ult}) and the elastic modulus (E). To reach both the compliance of small-diameter coronary arteries (0.0725 %/mmHg) and a burst pressure of 2031 mmHg, a material with a minimum σ_{ult}/E ratio of 1.78 is required. Based on this result and on data from the literature, random electrospun Polyurethane/Polycaprolactone (PU/PCL) tubular scaffolds were fabricated and compared to commercial ePTFE prostheses. PU/PCL grafts showed mechanical properties close to those of native arteries, with a circumferential elastic modulus of 4.8 MPa and a compliance of 0.036 %/mmHg at physiological pressure range (80-120 mmHg) for a 145 µm-thick prosthesis. In contrast, commercial expanded polytetrafluoroethylene (ePTFE) grafts presented a high Young's modulus (17.4 MPa) and poor compliance of 0.0034 %/mmHg. The electrospun PU/PCL did not however reach the target values as its σ_{ult}/E ratio was lower than expected, at 1.54, well below the calculated threshold (1.78). The model tended to overestimate both the compliance and burst pressure, with the differences between the analytical and experimental results ranging between 13 and 34 %, depending on the pressure range tested. This can be explained by the anisotropy of random electrospun PU/PCL, which did not present a perfectly linear elastic behavior, in contrast to the hypotheses of our model. Impermeability tests showed that the electrospun scaffolds were impermeable to blood for all thicknesses above 50 µm. In conclusion, this analytical model allows to select materials with suitable mechanical properties for the design of small-diameter vascular grafts. The novel electrospun PU/PCL tubular scaffolds showed strongly improved compliance as compared to commercial ePTFE prostheses.

1 Introduction

Medical challenges associated with small-diameter vascular grafts (VG, Ø ≤ 6 mm) are well known in the cardiovascular field. Synthetic grafts are required when there are no autologous arteries or veins available for the replacement of diseased blood vessels. Commercial vascular grafts made from polyethylene terephthalate (PET) or expanded polytetrafluoroethylene (ePTFE) present favorable outcomes for large diameter arteries, but are prone to failure when used for small-diameter vessels [1-3]. This is mainly due to the absence of adequate endothelialisation on the lumen side of prostheses, as well as a mismatch of mechanical properties between these latter and native arteries, which will cause thrombosis and intimal hyperplasia, respectively [4, 5]. These complications could be mitigated by designing a graft with a material that matches the mechanical and structural properties of the native tissue as closely as possible. Many attempts have therefore been made to design vascular grafts with better compliance while maintaining a safe burst pressure [6]. Compliance is the capacity of the prosthesis to expand in the circumferential direction in response to a pulsatile pressure [7], while the burst pressure is the pressure that will cause the rupture of the prosthesis. The compliance of a human coronary artery at the physiological pressure range is 0.0725 %/mmHg [8] and the burst pressure of a mammary artery is 2031 mmHg [9]. These should be the target values when designing small-diameter VG for coronary arteries replacement. Although promising work has been performed in a bid to find new biomaterials, to the best of our knowledge, current prostheses are either unable to reach such target values of native arteries [10] or are difficult to assess, since the compliance and burst pressure are not specified or the materials have been validated using target values based on saphenous veins [11] or pork arteries [12, 13] instead of the genuine artery that is meant to be replaced.

In addition to the previous parameters, the wall thickness is a critical element in any VG design. It plays a key role in the compliance and burst pressure strength obtained. Indeed, attempts to reduce the wall thickness in order to increase compliance to the target values of native arteries [10, 14] can lead to reduced burst pressure, which may then be insufficient. The wall thickness also has an influence on blood permeability and graft handling by surgeons during implantations. Thus, obtaining an adequate balance between all mechanical properties and geometrical parameters, especially blood permeability, burst pressure and compliance, can be challenging when choosing the thickness of the prosthesis. In order to develop an approach that avoids trial and

error, there is a need for a versatile mathematical model that helps narrow the choice of material and optimize the geometry.

Electrospun mats are particularly interesting for such biomedical applications as human tissues are characterized by nanometric fibrous structures. Hence, electrospun fibers have shown their ability to mimic the morphology of biological systems [15, 16]. Moreover, the fiber diameter and porosity can be adjusted to promote cell interaction, favor cell invasion (or rather, limit cell penetration), for example, to form an endothelial monolayer on the lumen surface [17, 18].

The goal of this study was to develop an analytical model to serve as an easy tool to select materials for small-diameter VG design for the replacement of coronary arteries; this selection would be based on the prediction of the materials' compliance and burst pressure determined from the mechanical properties obtained from uniaxial tensile tests. The second aim of this work was to choose a proper material based on this model, fabricate electrospun tubular scaffolds, and then compare their in vitro performances with that of the commercial ePTFE prosthesis.

2 Materials and Methods

2.1 Analytical Model

The analytical model was created on Matlab® using the analytical formulas of an internally pressurised cylinder to calculate compliance and burst pressure [14, 19]. The formulas for thick cylinders were chosen instead of the easier thin cylinder model. With the latter being a simplification only suitable when the radius divided by the thickness gives a result of 10 or more [14], the more complete model was used to allow a wider range of prosthesis thicknesses in the analysis.

The intrinsic material properties entered in the model were the Poisson's ratio (ν) and the Young's modulus (E). Therefore, this model could be used for an isotropic material in the elastic region of its mechanical properties. The geometric parameters in the model were the internal radius (Ri) and the thickness (t) of the cylinder wall.

The external radius (Re) was calculated from "Ri" and "t" at rest (no internal pressure). The length of the cylinder was fixed, and its value didn't influence the results as this wasn't a variable in the calculations.

A pressure difference (dP) is applied uniformly inside the cylinder, and induces circumferential and radial stresses, respectively σ_C and σ_R. It also creates a longitudinal stress σ_L since the length is fixed. These three stresses are illustrated in Figure 1. The effective von Mises stress σ_e and the radial displacements are then calculated based on the preceding. The stresses and displacement can be obtained at any point in the thickness, according to equations 1-4 [14]:

$$\sigma_R = \frac{R_i^2 * dP}{R_e^2 - R_i^2} * \left(1 - \frac{R_e^2}{R_i^2}\right) \quad \text{Equation 1}$$

$$\sigma_C = \frac{R_i^2 * dP}{R_e^2 - R_i^2} * \left(1 + \frac{R_e^2}{R_i^2}\right) \quad \text{Equation 2}$$

$$\sigma_L = 2 * \mu * \frac{R_i^2 * dP}{R_e^2 - R_i^2} \quad \text{Equation 3}$$

$$\sigma_e = \frac{1}{\sqrt{2}} * \sqrt{(\sigma_R - \sigma_C)^2 + (\sigma_C - \sigma_L)^2 + (\sigma_L - \sigma_R)^2} \quad \text{Equation 4}$$

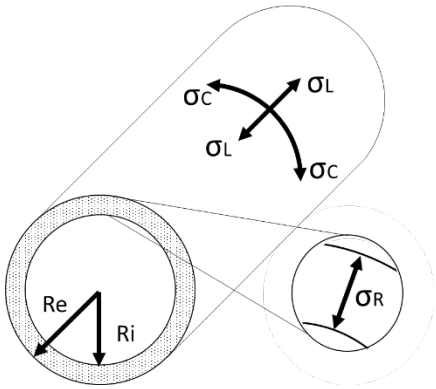

Figure 1 - Schematic illustration of stresses involved in the model calculation. σ_C, σ_R and σ_L represents respectively the circumferential stress, the radial stress and the longitudinal stress inside the cylinder with a fixed length and a uniformly applied internal pressure. The wall thickness t represents the difference between the external radius Re and the internal radius Ri.

(Single-column fitting image)

The compliance (C) is calculated following Equation 5, where dRi is the difference between the internal radius at the highest and the lowest pressures. The variation of internal pressure is always 40 mmHg. The compliance is expressed in %/mmHg.

$$C = \frac{dR_i}{R_i * dP} * 100 \qquad \text{Equation 5}$$

The model is also used to calculate the stress at burst pressure by changing the internal pressure to the target value of 2031 mmHg. The script was used with known material parameters (ν and E) and the thickness of the wall was iterated until the target compliance was reached. The stress at burst pressure was calculated from that thickness. This stress value represents the minimum ultimate stress (σ_{ult}) a material needs to be able to reach the target burst pressure. Each value of modulus was then associated with this stress value. Calculations were done for vascular grafts ranging from 3 to 6 mm in diameter.

2.2 Fabrication of Tubular Scaffolds

2.2.1 Materials

Thin wall ePTFE prostheses (Gore-Tex®, W. L. Gore & Associates, Flagstaff, U.S.A) were selected for their prevalence on the VG market. Polyurethane (PU, MDI-polyester/polyether polyurethane, CAS 68084-39-9), polycaprolactone (PCL, Mn = 80 000) and polyethylene oxide (PEO, viscosity average molecular weight Mv = 600 000) were purchased from Sigma-Aldrich Canada Co., as well as the chemicals, tetrahydrofuran (THF) and N,N-Dimethylformamide (DMF).

2.2.2 Electrospinning

PU/PCL (8 wt%) solutions were prepared by dissolving pellets consisting of 90 % PU/10 % PCL (w/w) in a 1:1 mix of THF and DMF. PU/PCL tubular scaffolds were produced on a 6-mm-diameter rotating mandrel using a homemade electrospinning setup. Table 1 presents the details of the electrospinning parameters for each solution. Parameters for the electrospinning of PU/PCL tubular scaffolds were optimized in order to obtain a similar morphology as PET mats previously developed by our team to limit EC invasion and reach a monolayer

of EC cells [17]. To facilitate unmolding of the prosthesis, a layer of PEO (0.5 mL of a 3 wt% PEO solution) was first electrospun on the mandrel. The unmolding process consisted in removing the PEO layer by immersing the mandrel in EtOH 50 % before recovering the PU/PCL tubular scaffold.

Table 1 - Process conditions used to produce electrospun tubular scaffolds

Material		Process parameters						Collector		Ambient	
Polymer	Concentration wt%	Tip-collector distance (cm)	Voltage (kV)	Flow rate (mL/h)	Needle size (G)	Needle translation (cm)	Translation speed (cm/s)	Ø (mm)	Linear velocity (cm/s)	RH (%)	Temp. (°C)
PU/PCL	8	20	12	0.15	21	11.6	2.2	6	3.8	19-29	22-25
PEO	3	20	30	2	18	22.5	2.2	6	3.8	19-21	22-25

2.3 Materials Characterization

Flat rectangular samples were cut from the tubular scaffolds for the characterization of their morphology and tensile properties.

2.3.1 Scaffolds morphology

Samples were sputter-coated with a 20 nm-thickness layer of chromium under vacuum. Electrospun nanofibers layouts were then evaluated by scanning electron microscopy (SEM) using a tabletop TM3030Plus instrument (Hitachi, Tokyo, Japan) at 15 kV. Images were analyzed using ImageJ (NIH, USA) software. Diameters were calculated based on about 200 different fibers from five different scaffolds. Pores were identified by an approximation of pores formed by fibers in a same plane in SEM images. The evaluation was done through two methods: (1) fitting polygonal pore shapes, allowing the calculation of the mean pore area; (2) manually fitting an ellipse inside the pore shape. The mean pore size is the average of the long and the short axis for each fitted ellipse. Calculations were made from twenty random measurements per image on ten different images.

2.3.2 Samples dimensions

Sample thicknesses were measured using a Progage Thickness Tester (Thwing-Albert Instrument Company, West Berlin, U.S.A.*).* Samples were sandwiched between two PET films to avoid errors due to compression. The length and width of each sample was measured using a caliper (Mitutoyo, Kawasaki, Japan).

2.3.3 Tensile tests

The tensile properties were evaluated using a uniaxial tensile testing machine (ElectroPuls E3000 from Instron, Norwood, U.S.A.) equipped with a 250 N load cell. Tensile tests were performed according to the ASTM D882-12 [20], with some modifications. The initial gage length was thus modified in order to maximize the potential elongation distance, and was set to 4.5 mm. As prescribed by the standard, the test speed was adjusted so that the strain rate of the sample would be 10 %/min. The width of the rectangular shape samples was kept to a minimum, at about 5 mm. As further compliance tests were performed in the wet state, mechanical properties were also tested after immersion in deionized water for 1 h for three different samples. Similar results were obtained for the dry state at room temperature, then experiments were performed in this latter condition. At least four different samples were tested in both the circumferential and longitudinal directions. The Young's modulus, tensile strength, and elongation at break were calculated using engineering stress-strain curves.

2.4 Vascular grafts characterization

Compliance, water permeability and burst strength were determined following the methods described in the standard ANSI/AAMI/ISO 7198:1998/2001/(R)2010 (Cardiovascular implants - Tubular vascular prostheses) [7].

2.4.1 Compliance

A tubular scaffold was installed in a bioreactor chamber on a TA Instrument® (New Castle, USA) Electroforce 3200 (see Figure 2). The scaffold was cannulated by inserting tube fittings into both ends and connecting the fittings to a reservoir filled with deionized water with a flow valve and gear and a peristaltic pump controlling

the pressure in the water system. The chamber was filled with deionized water to a constant level. An initial tension (between 0.3 N and 0.5 N) was applied longitudinally. The pulsatile intraluminal pressure was set at three different ranges (50-90, 80-120, 110-150 mmHg) during 90 cycles, as indicated in the ATSM standard [7]. The test was repeated three times for each scaffold. A laser measured the outer diameter of the scaffold subjected to pulsatile pressure changes, and the compliance was calculated using Equation 5. The thickness of the scaffold being low (< 500 µm), the wall was considered incompressible, and the internal diameter was obtained after subtracting two times the wall thickness from the outer diameter.

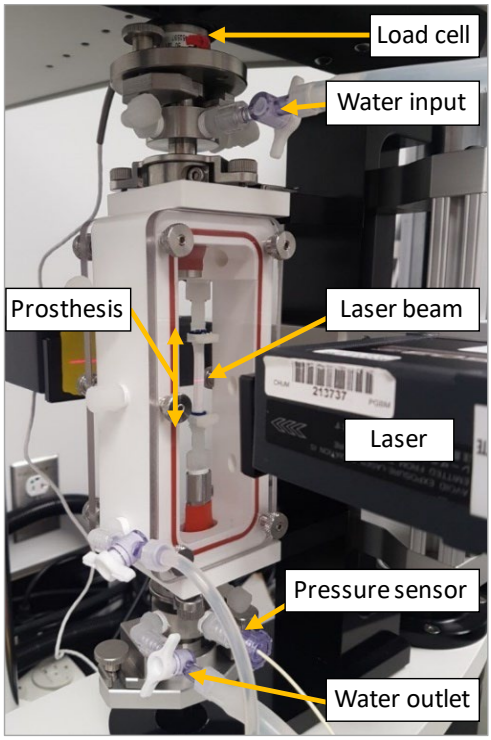

Figure 2 - Setup for VG compliance testing on the Electroforce 3200.

(Single-column fitting image)

2.4.2 Water permeability

The tubular scaffold was fitted in the bioreactor chamber similarly to what was done in the compliance test and connected to a water reservoir as well. The chamber was installed on a horizontal plane and a collector was placed below the scaffold. Water pressurized at 120 mmHg was circulated to the scaffold. The fluid permeating

through the graft was collected for 15 minutes. The graft permeability was determined using the following equation:

$$P_w = \frac{V}{A*d} \qquad \text{Equation 6}$$

Where P_w is the water permeability of the tubular scaffold (expressed in $mL.cm^{-2}.min^{-1}$), V is the permeated volume, A is the graft area allowing the permeation in the sample holder, and d is the duration of the test.

Tubular scaffolds of several thicknesses, between 30 and 200 µm, were evaluated for permeability to determine the minimum thickness to reach blood impermeability. The structural characteristics of filter materials such as the pore size and the thickness, the viscosity of the fluid and the interactions between the fluid and the material, are known to impact its permeability [21, 22]. De Valence et al. [23] evaluated both water and blood permeabilities through electrospun grafts. They reported that in vitro permeability values, respectively of 23.4 ± 5.1 $mL.cm^{-2}.min^{-1}$ and 0.16 ± 0.07 $mL.cm^{-2}.min^{-1}$, did not lead to blood leakage during in vivo implantations. These values were thus extrapolated as upper limits in order to guarantee blood impermeability for our scaffolds.

2.4.3 Burst pressure

Burst pressure experimental tests were performed using a closed air system. The tubular scaffold was cannulated through one extremity to a compressed air system and the other end was plugged. A manometer with a resolution of 0.5 psi (26 mmHg) was used to record the increasing pressure controlled manually. The test was run until the burst pressure was reached. A home-made latex balloon was used inside the prosthesis to prevent air loss through the porosity of the prosthesis. At least eight experiments were performed with prostheses of different thicknesses.

3 Results

3.1 Calculations from the Analytical Model

The cylindric analytical model was first used to identify the materials properties required to reach both the target compliance (0.0725 %/mmHg) and burst pressure (2031 mmHg) as a function of the geometry of the prosthesis. To that end, the material was considered (simplified) as an isotropic material characterized by its Young's modulus (E), Poisson's ratio (ν) and ultimate strength (σ_{ult}) in tension. Figure 3A presents the evolution of the minimum σ_{ult}/E as a function of the Ri/t ratio to reach these target values, according to Matlab® script. Changing the internal diameter of the prosthesis did not influence the results: as long as the target values were kept the same, the curves all superimposed perfectly, irrespective of the internal diameter of the prosthesis.

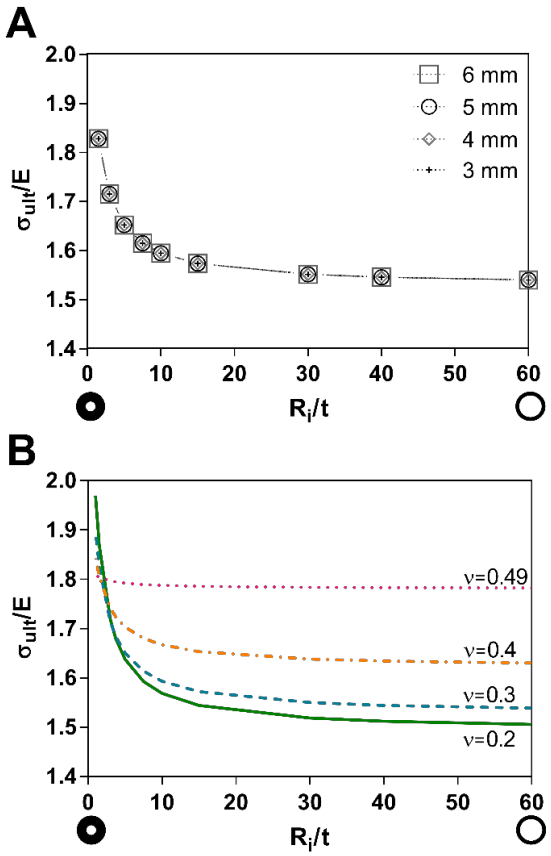

Figure 3 - (A) Lower limit of the ratio of tensile ultimate strength to elastic modulus (σ_{ult}/E) according to the ratio of the internal radius to wall thickness (Ri/t) to reach both compliance and burst pressure target values, respectively 0.0725 %/mmHg and 2031 mmHg. The Poisson's ratio was fixed as 0.3. Curves for VG with diameters of 3 to 6 mm are superposed. (B) Impact of Poisson's ratio value on the ratio of tensile strength to elastic modulus (σ_{ult}/E).

(Single-column fitting image)

The minimum σ_{ult}/E ratio was influenced both by the Poisson's ratio and the geometry of the cylinder. For small values of the R_i/t ratio, i.e., when the cylinder's radius was low as compared to its wall thickness, the minimum σ_{ult}/E ratio increased. Conversely, the curve tended to an asymptote when R_i/t increased. The influence of R_i/t was particularly strong for low Poisson's ratio values (Figure 3B). For a material close to being incompressible, with a Poisson's ratio as high as 0.49, the model showed almost no changes in the σ_{ult}/E results with a change in R_i/t, staying at around 1.78. However, when the Poisson's ratio was lower, the range of the results was wider and the value at the asymptote was lower, decreasing to up to 1.50, for a Poisson's ratio of 0.2. In order to meet small-diameter VG requirements, we must select a material at the very least capable of reaching the highest calculated value as σ_{ult}/E ratio. Thus, the ideal ratio is 1.78, which ensures the material is picked without knowing its Poisson's ratio, and is chosen as the minimum target ratio.

Based on this result, a literature search was performed to identify materials with mechanical values allowing the target burst pressure and compliance to be reached. We were particularly interested in electrospinning as a technique for producing nonwoven fibrous materials allowing tailored nanofiber morphology and porosity and capable of mimicking native tissues. Guo et al. [24] showed that electrospun PU/PCL mats presented an elastic modulus of 13.8 MPa with 60 MPa as tensile strength, leading to a σ_{ult}/E ratio of 4.36, which is even higher than our target. The second part of this work therefore focused on the fabrication and characterization of tubular scaffolds by electrospinning a PU/PCL material. Those scaffolds were compared with a commonly used ePTFE prosthesis in order to confirm the latter's potential for vascular grafts and the benefits of the analytical model.

3.2 Materials Characterization

3.2.1 Morphology

The morphology of ePTFE prostheses and PU/PCL electrospun tubular scaffolds, observed by SEM, are illustrated in Figure 4. ePTFE displayed a typical node-fibril microstructure (Fig. 4b-c) with more elongated fibrils for its outer layer, while PU/PCL scaffolds showed randomly oriented nanofibers with a mean diameter of 523 ± 93 nm (Fig. 4e-f). Their mean pore area was of 1.7 ± 1.0 μm^2, with the highest frequency for a small

pore area (under 2 μm^2). The mean pore diameter was also evaluated at 1.5 ± 0.8 µm with the fitting ellipse method (the average for the major axis and the minor axis are respectively 2.1 ± 0.9 µm and 1.0 ± 0.3 µm).

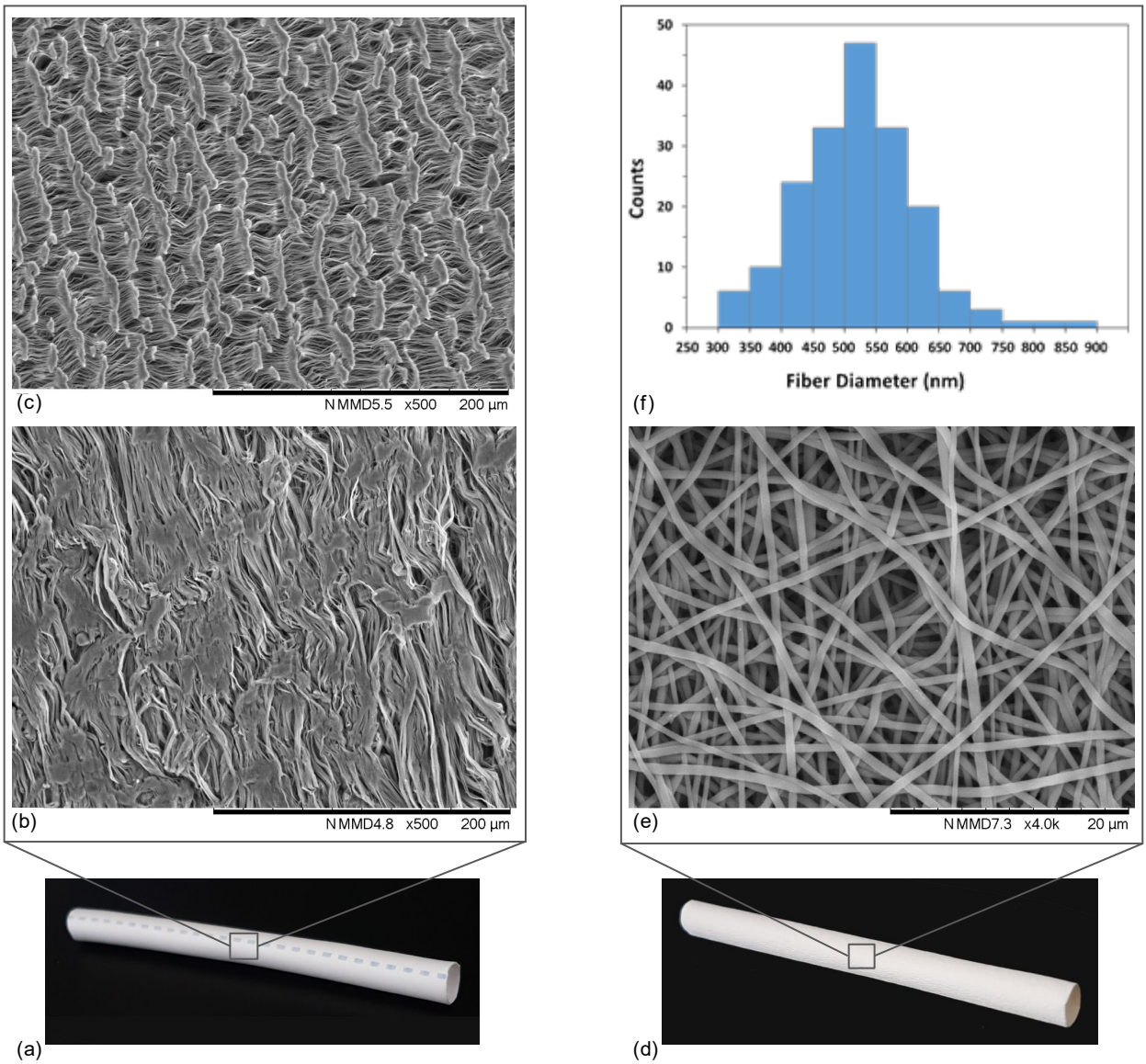

Figure 4 - Morphology of vascular prostheses: commercial ePTFE VG (left side, a-c) and electrospun PU/PCL tubular scaffold (right side, d-f). Digital images of respective VG (a, d). SEM images of (b) outer layer of the ePTFE VG, (c) inside layer of the ePTFE VG (scale bar: 200 µm), (e) electrospun PU/PCL nanofiber scaffolds (scale bar: 20 µm). (f) Distribution of PU/PCL fiber diameters according to ImageJ analyses.

(2-column fitting image)

3.2.2 Tensile properties

The mechanical properties of ePTFE prostheses and our electrospun PU/PCL tubular scaffolds were characterized by tensile testing. Mechanical properties obtained in both circumferential and longitudinal directions are presented in Figure 5.

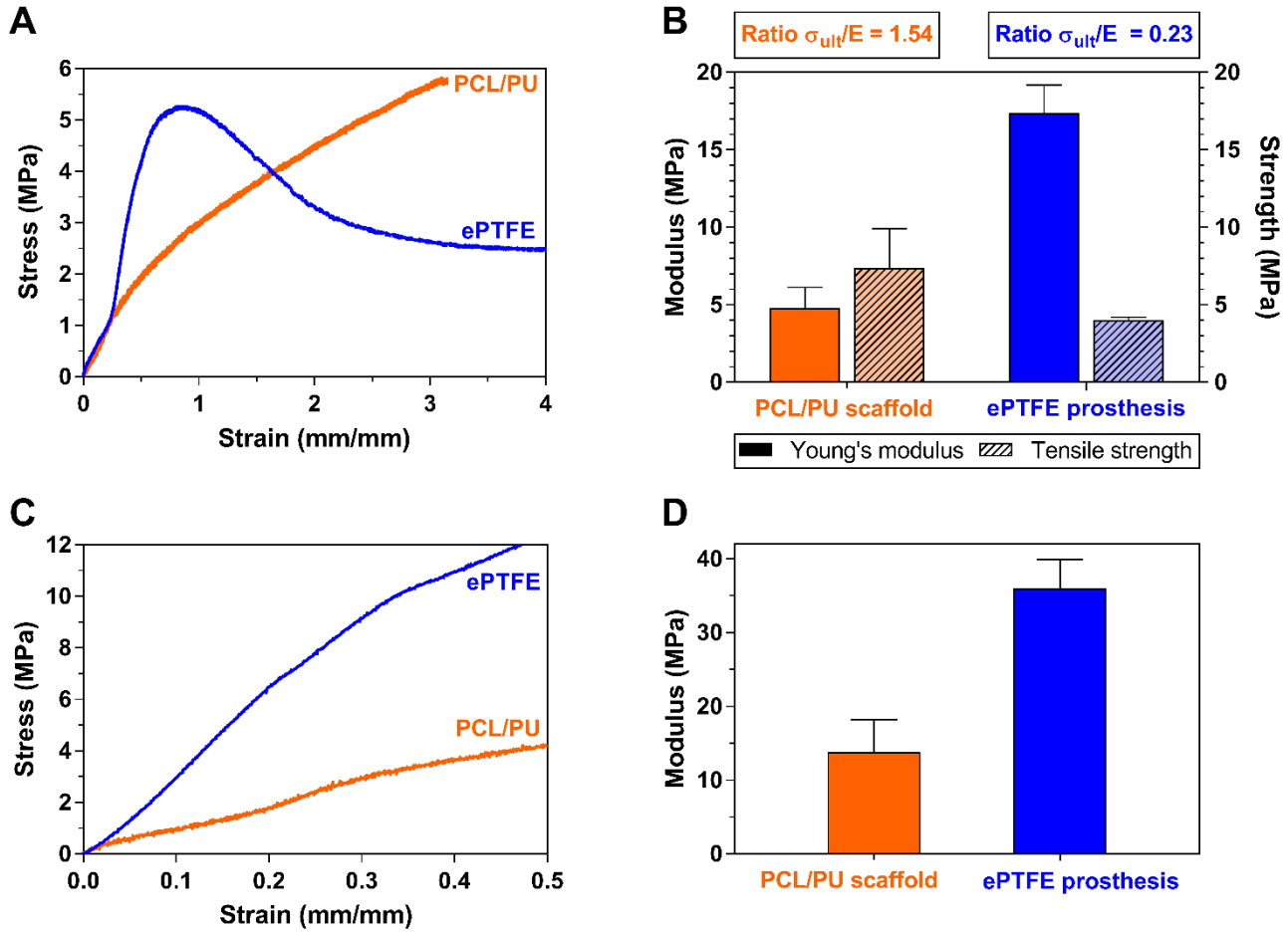

Figure 5 - Mechanical properties of PU/PCL electrospun tubular scaffolds and ePTFE commercial prosthesis, from tensile testing in (A, B) circumferential and (C, D) longitudinal directions. (A, C) Representative stress-strain curves. (B, D) Tensile properties: Young's modulus (E) from the initial stress-strain curve region and tensile strength (σ_{ult}), with value of the calculated ratio σ_{ult}/E. For the longitudinal direction, only the elastic modulus was calculated.

(2-column fitting image)

Commercial ePTFE VG exhibited a short linear region in the initial stress-strain curve (about ε = 0-25 %), with a low elastic modulus (4.4 ± 0.2 MPa), followed by a steeper slope (modulus of 17.4 ± 1.8 MPa), and then by a decrease indicating plastic deformation. In the longitudinal direction, ePTFE exhibited only one slope with a Young's modulus of 36.0 ± 3.9 MPa. Electrospun PU/PCL presented a quite linear behavior until rupture. This

mechanical behavior is consistent with previous work on electrospun PU/PCL and various polymer ratios between PCL and PU [24]. The Young's moduli of electrospun materials in the circumferential and longitudinal directions were respectively 4.8 ± 1.3 MPa and 13.8 ± 4.4 MPa. The circumferential σ_{ult} was 7.4 ± 2.5 MPa. The σ_{ult}/E ratio of PU/PCL and ePTFE materials were calculated as 1.54 and 0.23, respectively, based on their circumferential elastic moduli.

The relatively anisotropic character of PU/PCL despite generally random nanofiber orientations, as well as the variability of the results, can be explained by the fact that the mechanical response of such electrospun structures is strongly affected by their morphology: only a fraction of fibers in the load direction is recruited and aligned during tensile tests, and the mechanical response is a function of their number [25, 26].

3.3 Vascular Grafts Characterization

3.3.1 Compliance

Compliance tests were carried out on the 0.45 mm-thick ePTFE prosthesis and on electrospun scaffolds of different thicknesses. Tensile testing was also performed on these samples to determine their Young's moduli and compare the experimental compliance values to theoretical ones calculated using the analytical model. The Poisson's ratio was assumed to be 0.46 for ePTFE VG [27, 28] and 0.48 for PU/PCL scaffold assessments [29]. However, the effective Poisson's ratios were not verified and, notably, it is well-known that porous materials properties cannot be predicted analytically due to their random structure [30]. Since two slopes had been observed during ePTFE tensile tests, the highest Young's modulus (17.4 MPa) was used during analytical calculations as it was found more representative of the compliance behavior of ePTFE according to equation 7, which links the modulus and the compliance for a simple thin wall cylinder [31]:

$$C = \frac{D_i}{2*E*t} \qquad \text{Equation 7}$$

Figure 6A summarizes the experimental and theoretical compliance values for both materials in the 80-120 mmHg range, while Table 2 presents the values at each pressure range tested (50-90; 80-120 and 110-150 mmHg, according to the ASTM standard [7].

At the physiological pressure range (80-120 mmHg), thick commercial ePTFE prostheses displayed a very low compliance of 0.0034 ± 0.0004 %/mmHg, in accordance with the analytical model (0.004 %/mmHg). In comparison, electrospun samples showed about 10-fold increase of the compliance, with 0.0360 ± 0.0018 %/mmHg for 145 µm-thick electrospun samples at the same pressure range. The model tended to overestimate the compliance of PU/PCL prostheses, with all the calculated analytical values being above the experimental results, as shown in different ways in Fig. 6A and 6B.

For each VG, it can be seen that the relative differences between experimental and analytical values were larger when the pressure range increased. In particular, the analytical model predicted only very slight changes in compliance values between the three pressure levels, while experimental data showed a clear decrease when the pressure range increases (Table 2). The difference between analytical and experimental data decreased when the thickness of VG increased (Fig. 6B). On average, PU/PCL results revealed relative adequacy, with a discrepancy of about 13 % between the model forecast and the reality for pressure levels of 50-90 mmHg. With higher pressure ranges of 80-120 mmHg and 110-150 mmHg, the results showed larger differences (respectively 25 % and 34 %).

Table 2 - Compliance values for commercial ePTFE prosthesis and electrospun PU/PCL VG. Comparison between the experimental results and theoretical values obtained from the analytical model calculation. Graphical representation of the 80-120 mmHg pressure range is shown in Figure 6A.

Material	**Commercial ePTFE prosthesis**			**Electrospun PU/PCL VG**		
Thickness (µm)	454 ± 4			145 ± 2		
Pressure range (mmHg)	50-90	80-120	110-150	50-90	80-120	110-150
Compliance from analytical model (%/mmHg)	0.0040 ± 0.0004	0.0040 ± 0.0004	0.0040 ± 0.0004	0.0517 ± 0.0047	0.0509 ± 0.0046	0.0502 ± 0.0044
Experimental compliance (%/mmHg)	0.0036 ± 0.0010	0.0034 ± 0.0004	0.0033 ± 0.0005	0.0430 ± 0.0024	0.0360 ± 0.0018	0.0318 ± 0.0010

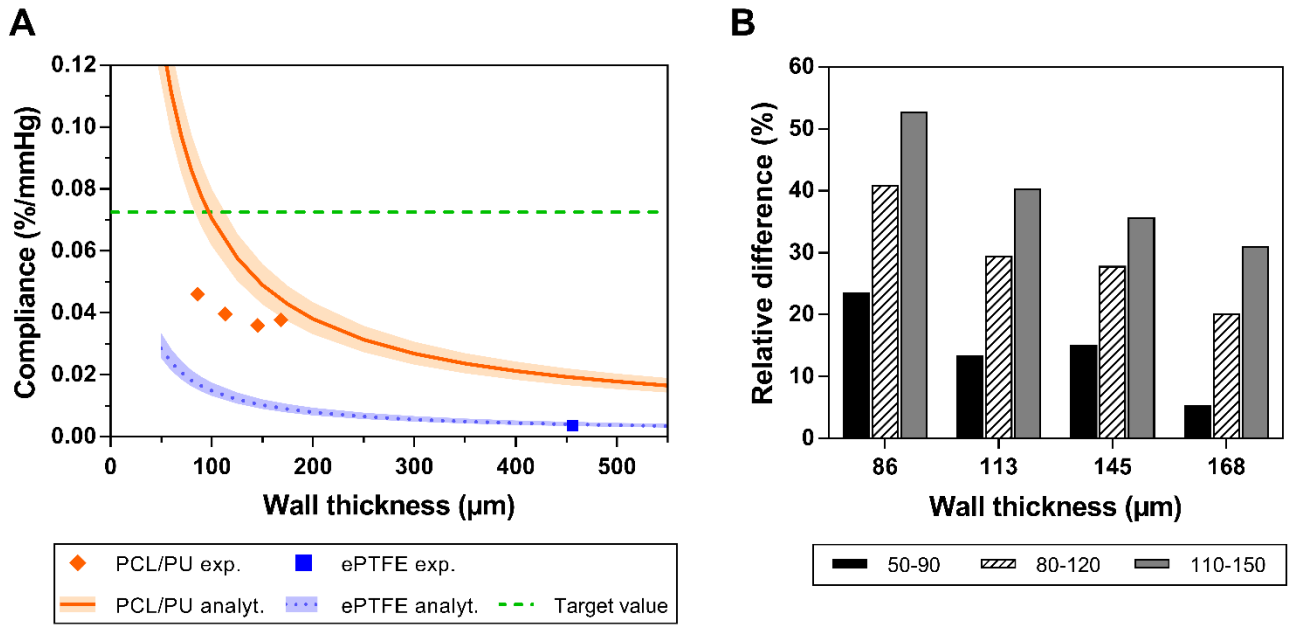

Figure 6 - Comparison of VG analytical and experimental compliance, as a function of wall thickness. (A) At the 80-120 mmHg pressure range. The fragmented line represents the compliance target value for small-diameter arteries (0.0725 %/mmHg). Experimental compliance values for PU/PCL prostheses are plotted (diamond). Their mean modulus (E = 3.9 MPa) was used to calculate the theoretical compliance for PU/PCL (plain curve). The colored area from either side corresponds to the minimum and maximum modulus of the tested prostheses. Similarly, the square and the dotted line, surrounded by the blue area, are respectively the experimental result (t = 454 ± 4 µm; E = 17.4 ± 1.8 MPa) and the analytical curve (E = 17.4 MPa) for ePTFE grafts. (B) Relative differences between experimental and analytical compliance data for PU/PCL VG (n = 6) at each pressure range tested (in mmHg).

(2-column fitting image)

3.3.2 Burst pressure

Burst pressure measurements were performed on electrospun PU/PCL scaffolds (Figure 7A). ePTFE prostheses were not tested, as expected values would have exceeded our equipment's capacity. The burst pressure experimental values followed an increasing tendency with the thickness, in accordance with the prediction of the analytical model. However, analytical values calculated using the ultimate stress determined during tensile testing were found to overestimate the burst pressure as compared to experimental measurements. Only one VG could reach the target value of 2031 mmHg, for a thickness of about 140 µm.

3.3.3 Permeability

Since a compromise may be needed between the compliance (increased at thinner wall thicknesses) and burst pressure (increased for thicker wall thicknesses), it is important to define which thickness is sufficient to ensure impermeability of the electrospun graft. To that end, the permeability of PU/PCL grafts was tested using a water leak test for a wide range of wall thicknesses. The results are summarized in Figure 7B and show that all our tested scaffolds manifested water leakage under the upper limit value of 23.4 mL.cm^{-2}.min^{-1}, and could be considered blood-impermeable and suitable for implantation. Very low permeability (< 0.6 mL.cm^{-2}.min^{-1}) was indeed obtained for graft thicknesses above the threshold of 50 µm.

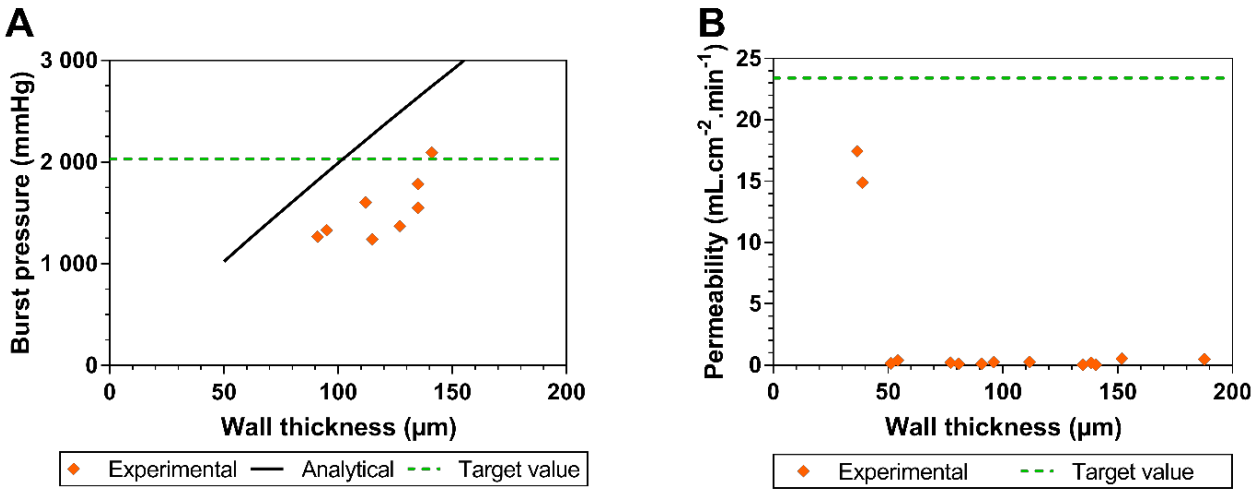

Figure 7 - Impact of wall thickness on (A) burst pressure and (B) water permeability, for electrospun PU/PCL tubular scaffolds. Each dot represents a distinct VG. The dotted line corresponds to (A) the target value for the burst pressure for small-diameter arteries (2031 mmHg [9]), (B) the upper limit of water permeability considered for blood-impermeable VG (23.4 mL.cm^{-2}.min^{-1} [23]). The theoretical value for burst pressure as a function of VG thickness is depicted by the dark line (A).

(2-column fitting image)

4 Discussion

Numerous materials have been investigated for the design of VG for the replacement of small-diameter arteries, but it is generally unclear whether they can avoid compliance mismatch, which is known to be related to hyperplasia and VG occlusion. The analytical model developed in this study allows to anticipate the ability of a material to mimic the compliance of the blood vessel to be replaced (0.0725 %/mmHg for a coronary artery) without the risk of burst rupture (2031 mmHg), based on the ultimate stress, the Young's modulus and the Poisson's ratio, available from tensile testing or directly from literature data.

A comparable approach was recently published [10], with the difference from our approach being that in theirs, the conically modified von Mises criterion was used instead of the von Mises effective stress. This criterion considers the compressive strength of the material under study and requires further tests. Since the compression behavior of electrospun materials is rarely reported, our model was designed to be as simple as possible in order to be used for wider purposes.

The σ_{ult}/E ratio defined by our analytical model is impacted by the Poisson's ratio. To be valid for any given Poisson's ratio, the σ_{ult}/E ratio should minimally reach 1.78 in order to meet small-diameter VG requirements. We therefore identified electrospun PU/PCL 90/10%, which had been reported to exhibit a σ_{ult}/E ratio of 4.36 [24], which is well above our target value. The electrospinning technique is particularly attractive as it produces nanofibrous materials mimicking native tissues' morphology [18, 32, 33]. The electrospinning parameters used for the fabrication of PU/PCL tubular scaffolds were adjusted to reach a morphology similar to that of electrospun PET prepared in our previous works [34], i.e., with nanofiber diameter around 500 nm and mean pore size of about 3 µm. The PU/PCL electrospun scaffolds had similar fiber diameters (523 ± 93 nm versus 551 + 91 nm) and even smaller pore diameters (1.5 ± 0.8 µm versus 3.2 ± 0.5 µm) than PET mats. According to our prior results, this morphology prevents the invasion of endothelial cells inside the structure, and therefore favors the formation of an endothelial monolayer on the lumen surface. This represents an advantage over ePTFE prostheses, whose structure allows cells to infiltrate in vivo through their pores, thus preventing the growth of a continuous endothelial monolayer on their surface [2, 3].

Morphological parameters of the PU/PCL scaffolds however differed from those of Guo et al. [24], which inspired our research, and whose average fiber diameter was 730 nm. This at least partly explains the difference in mechanical properties observed between our scaffolds and those of Guo et al. [24]: we obtained an elastic modulus closer to that of native arteries (4.8 MPa),with a 7.3 MPa tensile strength; this is much lower than the values reported by Guo et al., namely, 13.8 MPa and 60 MPa for modulus and ultimate stress, respectively. Therefore, our calculated σ_{ult}/E ratio was 1.54, much smaller than that of Guo et al. (4.36) and slightly lower than the 1.78 target value. This could explain why the experimental compliance of the 145 µm-thick prosthesis, which had sufficient burst resistance, was below the target value of 0.0725 %/mmHg reported as the compliance of small-diameter arteries [8], to wit 0.0360 %/mmHg.

Nevertheless, the compliance of PU/PCL VG was 10 times higher than that of commercial ePTFE prostheses, which was only 0.0034 %/mmHg, i.e., about 20 times smaller than the target value. The low compliance was consistent with values described in the literature for ePTFE prostheses, where Gore-Tex® and Impra® are shown to exhibit compliance values from 0.0026 [35] to 0.009 [36] and 0.012 %/mmHg [37, 38]. Furthermore, experimental results were in accordance with the analytical model, when considering the second slope of the stress-strain curves for the circumferential direction of ePTFE material, which exhibited a change in the slope after about 25 % of strain. This difference in elastic modulus as a function of the elongation state was corroborated by Jia et al. [39] for another ePTFE VG : the modulus changed from 8.6 MPa at 10 % strain to 32.1 MPa at 30 %. It is believed that this inflexion is due to the tubular origin of the samples tested, leading to residual stress - at the beginning of the tensile test, the thin external layer is in compression, while the internal layer is already in tension. Hence, when the tensile test starts, the fibrils from the outer layer began to elongate before those from the inner layer start to get involved in the test direction. To verify this hypothesis, SEM imaging was performed at different elongated states of ePTFE. At 10 % strain, the fibrils of the external layers were indeed more elongated than at the rest state, while no change was observed at the internal side of ePTFE grafts. This emphasizes the importance of testing VG without cutting and using specific grips, according to the ANSI 7198 standard [7].

Despite being presented as a “thin wall” in the catalog of VG suppliers, the ePTFE prostheses used in the present study had a wall thickness above 400 µm. Decreasing the thickness could allow a slight increase of the

compliance. However, this would lead to decreased resistance to burst pressure. According to our analytical model (Figure 6A), the mechanical properties in tension would not allow both the compliance and burst resistance to be reached. In contrast, electrospun PU/PCL materials should be able to meet the target compliance for wall thicknesses under 100 µm. Although this seems sufficient for blood impermeability, it would make handling more difficult during production and surgery. Moreover, the burst pressure would be below the value of 2031 mmHg (Figure 7A) chosen based on the burst pressure resistance of mammary arteries [9]. This target value could however be decreased for prosthesis design, since it is well above physiological pressures, being 10 times higher than the pressure that can be reached in hypertension [9].

Based on experimental and analytical results, a 140 µm-thick electrospun PU/PCL tubular scaffold could represent a good compromise as a VG in terms of easy handling, appropriate blood impermeability, high burst pressure and a compliance greater than the commercial ePTFE prosthesis.

The analytical model developed in this study however has several limitations. Relative differences between analytical calculations and experimental compliance results were evaluated to be up to 13 % at the 50-90 mmHg pressure range, and increased for higher pressure range to up to 34 %. Overall, the model made an overestimation of the compliance and burst pressure. Our model predicts mechanical properties assuming the presence of isotropic materials with linear elastic behavior. This is a major drawback as polymers generally exhibit at least slightly non-linear behavior and viscoelasticity. Moreover, both the ePTFE material and electrospun PU/PCL scaffolds revealed a larger Young's modulus in the longitudinal direction than in the circumferential direction, showing an unexpected anisotropic character. These limitations could partially explain the differences between the model and experimental values. An orthotropic model could enable to reach more realistic values.

The tendency of these differences to be higher with smaller thicknesses could be explained with the method used to measure the thicknesses, as it required the compression of samples, and an error always has a greater impact on small values. Furthermore, in designing this simplified model, assumptions were made that did not exactly fit the experimental reality. Indeed, the internal radius variation remained the same in the calculations irrespective of the pressure, while the initial radius increased with higher pressure ranges and resulted in a lower compliance value according to Equation 5. Input parameters such as the elastic modulus and the wall thickness

were also kept fixed in the model, but could also change experimentally depending on the pressure applied on the scaffold and the mechanical behavior [40].

Interestingly, PU/PCL scaffolds showed a reduction of the compliance at higher pressures, which represents a behavior close to that of native arteries [40]. This behavior is known to be due to the fact that in arteries, elastin is much more flexible than collagen, and elastin fibres from the tunica media are stretched before collagen fibres which are mainly in the external layer. This leads to a non-linear behavior in compliance [3, 41, 42].

5 Conclusion

In conclusion, a simple analytical model tool for the prediction of compliance and burst pressure of vascular grafts based on their mechanical properties in tension was developed and validated. This model could be greatly useful in selecting an appropriate material for the design of small-diameter prostheses. Electrospun PU/PCL was identified as a promising material. A 145 µm-thick tubular scaffold presented an adequate burst resistance and permeability and a compliance of 0.036 % mmHg, a clear improvement over those of current vascular replacement solutions such as ePTFE.

Acknowledgements

This research was supported by the Natural Sciences and Engineering Research Council of Canada (NSERC) and the Canadian Institutes of Health Research (CIHR) (CPG 127764) as well as the Canada Research Chair in biomaterials and endovascular implants (CRC, 950-229036). Mélusine Bouchet gratefully acknowledges scholarships from École de Technologie Supérieure. The authors also thank Cercle Cerclé (École Polytechnique) and Boris Chayer (CRCHUM) for their skilled technical support.

References

[1] M.J. McClure, P.S. Wolfe, I.A. Rodriguez, G.L. Bowlin, Bioengineered vascular grafts: Improving vascular tissue engineering through scaffold design, Journal of Drug Delivery Science and Technology, 21(3) (2011) 211-227.
[2] J. Chlupác, E. Filová, L. Bacáková, Blood Vessel Replacement: 50 years of Development and Tissue Engineering Paradigms in Vascular Surgery, Physiological Research, 58(2) (2009) S119-S139.
[3] C. Singh, C.S. Wong, X. Wang, Medical Textiles as Vascular Implants and Their Success to Mimic Natural Arteries, Journal of functional biomaterials 6(3) (2015) 500-525.
[4] W.M. Abbott, J. Megerman, J.E. Hasson, G. L'Italien, D.F. Warnock, Effect of compliance mismatch on vascular graft patency, Journal of Vascular Surgery, 5(2) (1987) 376-382.
[5] S.F.C. Stewart, D.J. Lyman, Effects of a vascular graft/natural artery compliance mismatch on pulsatile flow, Journal of Biomechanics, 25(3) (1992) 297-310.
[6] M. Desai, A.M. Seifalian, G. Hamilton, Role of prosthetic conduits in coronary artery bypass grafting, European Journal of Cardio-thoracic Surgery, 40(2) (2011) 394-398.
[7] American National Standards Institute, ANSI/AAMI/ISO 7198:1998/2001/(R)2010, Cardiovascular implants - Tubular vascular prostheses, Association for the Avancement of Medical Instrumentation, 2010, p. 56.
[8] J.A. Shaw, B.A. Kingwell, A.S. Walton, J.D. Cameron, P. Pillay, C.D. Gatzka, A.M. Dart, Determinants of coronary artery compliance in subjects with and without angiographic coronary artery disease, Journal of the American College of Cardiology, 39(10) (2002) 1637-1643.
[9] N. L'Heureux, N. Dusserre, G. Konig, B. Victor, P. Keire, T.N. Wight, N.A.F. Chronos, A.E. Kyles, C.R. Gregory, G. Hoyt, R.C. Robbins, T.N. McAllister, Human tissue-engineered blood vessels for adult arterial revascularization, Nat. Med. 12(3) (2006) 361-365.
[10] O. Castillo-Cruz, C. Perez-Aranda, F. Gamboa, J.V. Cauich-Rodriguez, D. Mantovani, F. Aviles, Prediction of circumferential compliance and burst strength of polymeric vascular grafts, Journal of the Mechanical Behavior of Biomedical Materials, 79 (2018) 332-340.
[11] A. Yin, K. Zhang, M.J. McClure, C. Huang, J. Wu, J. Fang, X. Mo, G.L. Bowlin, S.S. Al-Deyab, M. El-Newehy, Electrospinning collagen/chitosan/poly(L-lactic acid-co-epsilon-caprolactone) to form a vascular graft: mechanical and biological characterization, Journal of Biomedical Materials Research Part A, 101(5) (2013) 1292-301.
[12] Z. Tan, H. Wang, X. Gao, T. Liu, Y. Tan, Composite vascular grafts with high cell infiltration by co-electrospinning, Materials Science and Engineering C, 67 (2016) 369-377.
[13] C. Li, F. Wang, G. Douglas, Z. Zhang, R. Guidoin, L. Wang, Comprehensive mechanical characterization of PLA fabric combined with PCL to form a composite structure vascular graft, Journal of the Mechanical Behavior of Biomedical Materials, 69 (2017) 39-49.
[14] A. Bazergui, A. Bui-Quoc, A. Biron, G. MacIntyre, C. Laberge, Résistance des matériaux, 3ème édition, Presses internationales Polytechnique, Montréal, 2002, pp. 220;392-398.
[15] Z.-M. Huang, Y.-Z. Zhang, M. Kotaki, S. Ramakrishna, A review on polymer nanofibers by electrospinning and their applications in nanocomposites, Composites Science and Technology, 63 (2003) 2223–2253.
[16] G. Zanatta, D. Steffens, D.I. Braghirolli, R.A. Fernandes, C.A. Netto, P. Pranke, Viability of mesenchymal stem cells during electrospinning, Brazilian Journal of Medical and Biological Research 45(2) (2012) 125-130.
[17] H. Savoji, M. Maire, P. Lequoy, B. Liberelle, G. De Crescenzo, A. Ajji, M.R. Wertheimer, S. Lerouge, Combining Electrospun Fiber Mats and Bioactive Coatings for Vascular Graft Prostheses, Biomacromolecules, 18(1) (2017) 303-310.
[18] A. Hasan, A. Memic, N. Annabi, M. Hossain, A. Paul, M.R. Dokmeci, F. Dehghani, A. Khademhosseini, Electrospun scaffolds for tissue engineering of vascular grafts, Acta Biomaterialia, 10(1) (2014) 11-25.
[19] M. Gauthier, A. Ajji, S. Lerouge, Conception et optimisation d'une prothèse artérielle multicouche composée de tissu électrofilé, École de technologie supérieure, Montréal, 2016.
[20] ASTM International, ASTM D882-12, Standard Test Method for Tensile Properties of Thin Plastic Sheeting, 2012.
[21] J. Geens, B. Van der Bruggen, C. Vandecasteele, Transport model for solvent permeation through nanofiltration membranes, Separation and Purification Technology 48(3) (2006) 255-263.

[22] D.R. Machado, D. Hasson, R. Semiat, Effect of solvent properties on permeate flow through nanofiltration membranes. Part II. Transport model, Journal of Membrane Science 166(1) (2000) 63-69.
[23] S. de Valence, J.C. Tille, J.P. Giliberto, W. Mrowczynski, R. Gurny, B.H. Walpoth, M. Möller, Advantages of bilayered vascular grafts for surgical applicability and tissue regeneration, Acta Biomaterialia 8(11) (2012) 3914-3920.
[24] F. Guo, N. Wang, L. Wang, L. Hou, L. Ma, J. Liu, Y. Chen, B. Fan, Y. Zhao, An electrospun strong PCL/PU composite vascular graft with mechanical anisotropy and cyclic stability, Journal of Materials Chemistry A, 3(9) (2015) 4782-4787.
[25] C.-L. Pai, M.C. Boyce, G.C. Rutledge, On the importance of fiber curvature to the elastic moduli of electrospun nonwoven fiber meshes, Polymer, 52(26) (2011) 6126-6133.
[26] M.S. Rizvi, P. Kumar, D.S. Katti, A. Pal, Mathematical model of mechanical behavior of micro/nanofibrous materials designed for extracellular matrix substitutes, Acta Biomaterialia, 8(11) (2012) 4111-4122.
[27] P.J. Rae, D.M. Dattelbaum, The properties of poly(tetrafluoroethylene) (PTFE) in compression, Polymer 45(22) (2004) 7615-7625.
[28] DuPont Fluoroproducts, Teflon® PTFE, Properties Handbook, Technical Report H-37051-3, DuPont, USA, p. 38.
[29] H.J. Qi, M.C. Boyce, Stress–strain behavior of thermoplastic polyurethanes, Mechanics of Materials, 37(8) (2005) 817-839.
[30] J. Kováčik, Correlation Between Elastic Modulus, Shear Modulus, Poisson's Ratio and Porosity in Porous Materials, Advanced Engineering Materials, 10(3) (2008) 250-252.
[31] Y. Chen, X. Ding, Y.L. Li, X.Q. Zhao, J.Y. Hu, Experimental Models of Compliance and Young's Modulus of Woven Vascular Prosthesis, Advanced Materials Research, 332-334 (2011) 609-612.
[32] A. Hadjizadeh, A. Ajji, M. Jolicoeur, B. Liberelle, G. De Crescenzo, Effects of Electrospun Nanostructure versus Microstructure on Human Aortic Endothelial Cell Behavior, Journal of Biomedical Nanotechnology, 9 (2013) 1159-1209.
[33] C. Rüder, T. Sauter, K. Kratz, T. Haase, J. Peter, F. Jung, A. Lendlein, D. Zohlnhöfer, Influence of fibre diameter and orientation of electrospun copolyetheresterurethanes on smooth muscle and endothelial cell behaviour, Clinical Hemorheology and Microcirculation, 55(4) (2013) 513-522.
[34] H. Savoji, A. Hadjizadeh, M. Maire, A. Ajji, M.R. Wertheimer, S. Lerouge, Electrospun nanofiber scaffolds and plasma polymerization: a promising combination towards complete, stable endothelial lining for vascular grafts, Macromolecular Bioscience, 14(8) (2014) 1084-1095.
[35] M.J. Moreno, A. Ajji, D. Mohebbi-Kalhori, M. Rukhlova, A. Hadjizadeh, M.N. Bureau, Development of a compliant and cytocompatible micro-fibrous polyethylene terephthalate vascular scaffold, Journal of biomedical materials research. Part B, Applied biomaterials 97(2) (2011) 201-214.
[36] N.R. Tai, H.J. Salacinsky, A. Edwards, G. Hamilton, A.M. Seifalian, Compliance properties of conduits used in vascular reconstruction, British Journal of Surgery, 87(11) (2000) 1516-1524.
[37] K.C. Hanel, C. McCabe, W.M. Abbott, J. Fallon, J. Megerman, Current PTFE grafts: a biomechanical, scanning electron, and light microscopic evaluation, Annals of Surgery, 195(4) (1982) 456-463.
[38] T.V. How, Mechanical Properties of Arteries and Arterial Grafts, in: G.W. Hastings (Ed.), Cardiovascular Biomaterials, Springer London, London, 1992, pp. 1-35.
[39] Y. Jia, Y. Qiao, I. Ricardo Argueta-Morales, A. Maung, J. Norfleet, Y. Bai, E. Divo, A.J. Kassab, W.M. DeCampli, Experimental Study of Anisotropic Stress/Strain Relationships of Aortic and Pulmonary Artery Homografts and Synthetic Vascular Grafts, Journal of Biomechanical Engineering, 139(10) (2017) 101003-1 - 101003-10.
[40] D. Suarez Bagnasco, F. Montini Ballarin, L.J. Cymberknop, G. Balay, C. Negreira, G.A. Abraham, R.L. Armentano, Elasticity assessment of electrospun nanofibrous vascular grafts: A comparison with femoral ovine arteries, Materials Science and Engineering: C, 45 (2014) 446-454.
[41] H.J. Salacinski, S. Goldner, A. Giudiceandrea, G. Hamilton, A.M. Seifalian, A. Edwards, R.J. Carson, The Mechanical Behavior of Vascular Grafts: A Review, Journal of Biomaterials Applications, 15(3) (2001) 241-278.
[42] G.S. Kassab, Biomechanics of the cardiovascular system: the aorta as an illustratory example, Journal of the Royal Society Interface, 3(11) (2006) 719-740.